Beslier, M.-O., Whitmarsh, R.B., Wallace, P.J., and Girardeau, J. (Eds.)
Proceedings of the Ocean Drilling Program, Scientific Results Volume 173

1. Data Report: Downcore Variation of Site 1068 Breccia Matrix Mineralogy[1]

Kristen E.K. St. John[2]

INTRODUCTION

Mass-wasting deposits characterize the Upper Jurassic(?) to Lower Cretaceous sedimentary record of the Iberia Abyssal Plain. These deposits include olistostromes at Site 897 (Shipboard Scientific Party, 1994a; Comas et al., 1996), olistostromes and/or possible rock-fall deposits at Site 899 (Shipboard Scientific Party, 1994b; Comas et al., 1996; Gibson et al., 1996), a breccia succession at Site 1068, slumped and fractured deposits at Site 1069, and a breccia succession at Site 1070 (Whitmarsh, Beslier, Wallace, et al., 1998). Whereas the exact origin of these deposits is uncertain, the regional common occurrence of middle to upper Mesozoic mass-wasting deposits suggests that they record the early rifting evolution of the west Iberia margin.

In order to better understand the sedimentological and tectonic processes active during the early rifting evolution of the west Iberia margin, Leg 173 shipboard and postcruise studies (e.g., this study; Beard and Hopkinson, in press) have focused on characterizing the 42-m breccia succession at Site 1068. Designated lithostratigraphic Unit IV, the breccia succession was subdivided into three subunits based on qualitative downcore variations in matrix composition, brittle deformation characteristics, and the degree of hydrothermal overprint. A complete description of the subunits can be found in Shipboard Scientific Party (1998). It was recognized aboard ship that the breccia matrix at Site 1068 is not uniform throughout the breccia succession. Based on color differences and shipboard mineralogical analyses it was clear that the matrix of Subunit IVA was compositionally distinct from the matrix of Subunits IVB and IVC and from macroscopic clasts within Subunit IVA.

[1]St. John, K.E.K., 2000. Data report: Downcore variation of Site 1068 breccia matrix mineralogy. *In* Beslier, M.-O., Whitmarsh, R.B., Wallace, P.J., and Girardeau, J. (Eds.), *Proc. ODP, Sci. Results,* 173, 1–14 [Online]. Available from World Wide Web: <http://www-odp.tamu.edu/publications/173_SR/VOLUME/CHAPTERS/SR173_01.PDF>. [Cited YYYY-MM-DD]
[2]Department of Geology, Appalachian State University, Boone NC 29608, USA. stjohnke@appstate.edu

Initial receipt: 12 October 1999
Acceptance: 7 June 2000
Web publication: 3 October 2000
Ms 173SR-009

However, it was not clear if the finer grained material between larger clasts (i.e., the matrix) in Subunits IVB and IVC was compositionally distinct from the larger clasts, nor was it clear to what degree the matrix was hydrothermally altered along the breccia's vertical extent. Mineralogical analyses made aboard ship could not address these questions because, except in those cases where the matrix-to-clast ratio in the breccia was relatively high (e.g., interval 173-1068A-16R-3, 70–90 cm), X-ray diffraction (XRD) analyses were performed on powdered samples of combined matrix material (finer grained particles and cement) plus adjacent macroscopic clasts. The result of those analyses was downcore estimates of the bulk mineral composition of the Site 1068 breccia succession.

This data report presents both qualitative and semiquantitative results from XRD analyses of the breccia matrix at Site 1068. In this study the matrix is defined as the fine-grained particles (as viewed through a binocular microscope) plus cement. Results are based on analytical methods that aimed to isolate the desired matrix from larger clast contamination prior to XRD analyses. In addition, the breccia was sampled at a higher resolution than was conducted aboard ship, producing a more complete description of downcore matrix mineralogical changes. The data presented here may be used to (1) further justify the subunit designation of Unit IV made aboard ship, (2) help determine to what degree the matrix and the larger clasts (studied in thin section aboard ship; Shipboard Scientific Party, 1998) are compositionally distinct, (3) help identify the extent of hydrothermal fluid migration in the breccia, and (4) support the proposed shipboard hypothesis that the Site 1068 breccia succession resulted from multiple mass-wasting events (see "Lithostratigraphy" section in Shipboard Scientific Party, 1998).

MATERIALS AND METHODS

Sample locations were selected based on the following criteria: (1) to maximize the matrix volume per core sample, (2) to sample where major matrix color change occurs in the core (presumably indicating mineralogical differences), and (3) to provide at least one sample per 1.5 m of core. Forty-seven samples were analyzed from the 42-m breccia succession in Hole 1068A (Fig. F1). Of these, 15 were from Subunit IVA, 23 from Subunit IVB, and 9 from Subunit IVC. In addition, one sample was taken from the very base of the overlying Unit II sediments (note: there is no Unit III at Site 1068), in order to show the compositional change between the pelagic/hemipelagic sediments of Unit II and the breccia of Unit IV. Each sample was between ~5 and ~20 cm^3 in volume, depending on the relative proportion of matrix to clasts in the sample.

XRD of the matrix material required both that the matrix be isolated from the embedded clasts and that the matrix be powdered (Bish and Reynolds, 1989). Both of these goals were achieved by using a handheld vibrating drill (similar to a dental drill) to carefully powder and separate the desired matrix material from the remaining well-lithified, clast-rich breccia. Such fine-scale, detailed work was enabled by viewing the particular drilling area on each core sample through a binocular microscope. Drilling of each sample ceased when ~0.5 g of powdered matrix had been collected.

To obtain semiquantitative results, an internal standard of 10 wt% of boehmite (an aluminum oxyhydroxide) was added to each powdered matrix sample. Boehmite was mixed with each sample by gently grind-

F1. Distribution of matrix mineralogy, Site 1068, p. 7.

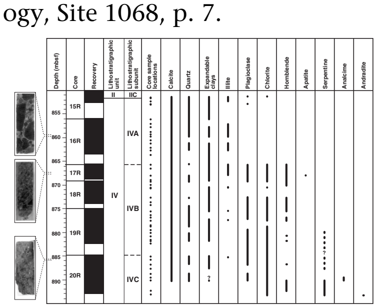

ing the mixture in acetone with a mortar and pestle and then air drying. Samples were backloaded into sample holders to obtain a random orientation of the mineral grains. If the volume of sample was insufficient to fill the sample holder, powdered gelatin was added as a backing. Because boehmite was added to each sample in a constant proportion, the integrated intensity ratio (i.e., peak area ratio) of a single mineral peak to the 6.11-Å boehmite peak can be used as an indicator of that mineral's abundance in the sample (Gibbs, 1967; Scheidegger and Krissek, 1982; Krissek, 1984, 1989; Krissek and Clemens, 1991; Krissek and Janecek, 1993). If samples were of uniform grain size and uniform composition, then calibration curves could be constructed to calculate mineral abundances from mineral/boehmite peak area ratios (Gibbs, 1967; Scheidegger and Krissek, 1982). The pressed powder samples of the breccia matrix at Site 1068, however, do not meet either of these conditions. Thus, calibration curves could not be constructed and the mineral/boehmite peak area ratios have not been converted to mineral abundances. Rather, downcore variations in the abundance of a single mineral (e.g., calcite) are described using downcore changes in the integrated intensity ratios of that mineral. This method does not allow for comparison of the absolute abundances of two or more different minerals.

Analytical precision was evaluated by analyzing five randomly selected replicate samples. The reproducibility estimates of the major mineral suite in the breccia matrix at Site 1068 are as follows (given as absolute mineral/boehmite peak area ratios): calcite (±0.11), quartz (±0.16), plagioclase (±0.03), chlorite (±0.33), hornblende (±0.01), and serpentine (±0.01). A previous study (Scheidegger and Krissek, 1982) has shown that absolute mineral abundances determined from mineral/boehmite peak area ratios using calibration curves are accurate at ±1% for quartz and plagioclase and at ±2% for chlorite. Mineral abundances inferred from peak area ratios measured in this study would have a lower accuracy than that cited above because of grain-size variations and the particular mineral suite present in each sample.

Samples were analyzed on a Shimadzu XRD-6000 X-ray diffractometer. Powder mounts were scanned at a rate of 0.5°/min with CuK_{α} radiation. Radiation was filtered using a 1° divergence slit, a 1° scatter slit, and a 0.15-mm receiving slit. Machine settings were 40 kV and 50 mA for all analyses. The generated raw data files were then computer processed to smooth data points (9-point smooth), remove amorphous background scatter, and remove the $K_{\alpha}2$ analytical spectrum component. Integrated intensities (i.e., peak areas) were calculated using a Shimadzu profile-fitting software package that performs mathematical modeling of the diffractogram pattern.

F2. XRD profiles of Site 1068 breccia matrix samples, p. 8.

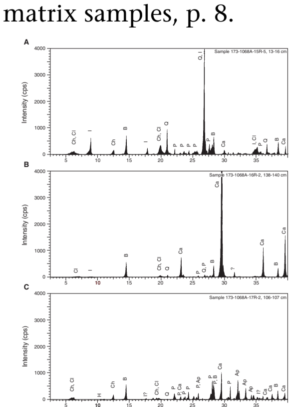

RESULTS

The downcore presence or absence of each mineral, or mineral group, identified from the diffractogram patterns is shown in Figure **F1**. Example diffractogram patterns of six samples are shown in Figure **F2**. Mineral peaks were generally sharp and well defined. The occurrence of broader peaks, such as at 5°–7°2θ, reflect the presence of various expandable clays, and at 32°–37°2θ, reflect the presence of serpentine minerals. The minerals present in the Site 1068 breccia matrix include: calcite, quartz, expandable clays, illite, plagioclase, chlorite, hornblende, apatite, analcime, serpentine, and andradite garnet. Distinguishing between albite and anorthite varieties of plagioclase was not possible given their similar 2θ peak positions. Clinochlore is the variety of chlorite that generally best matches the diffractogram pattern; however, the blue ferriferous chloride mineral aërinite was identified in Sample 173-1068A-20R-7, 24–26 cm. Hornblende varieties include ferrorichterite and ferropargasite. Apatite is the F-rich variety, fluorapatite. Serpentine varieties include lizardite and chrysotile. In addition, although the presence of the mineral brucite was indicated from shipboard XRD analyses (Unit I; Shipboard Scientific Party, 1998), it could not be identified in this study with any certainty because of an overlap in peak position with the higher 2θ boehmite peaks. A comparison between downcore trends in breccia matrix mineralogy determined from this study and the downcore trends in breccia bulk mineralogy as determined aboard ship are given in Table T1.

T1. Bulk and matrix compositions of breccia subunits, p. 12.

Downcore clay mineral abundance could not be quantified given the difficulty in distinguishing among the many possible clay mineral varieties when the clay minerals are not oriented, as is the case with pressed-powder samples. Further complicating the identification and quantification of clay minerals based on diffractogram patterns is the fact that the 14-Å chlorite peak lies at ~6.1°2θ, partially overlapping clay peaks with similarly high d-spacings. However, downcore changes in the shape of the 5°–7°2θ peak(s) indicate that a variety of clay types exist in the breccia matrix and that their abundance varies downcore. Figure F3 shows a sampling of the downcore change in the shape of the 5°–7°2θ peak and also the presence (or absence) of the 10-Å illite peak (8.8°2θ). Based on the position and shape of the 5°–7°2θ peak, montmorillonite (smectite) group minerals including, but not restricted to, 15-Å saponite and 15-Å nontronite are probably present in the matrix (Carroll, 1970). Saponite and nontronite can be produced from the hydrothermal alteration of mafic and ultramafic rocks including lherzolite (Velde, 1995), of which the basement rock underlying the breccia succession is partially composed (Shipboard Scientific Party, 1998). Alternatively, saponite and nontronite can form diagenetically (Velde, 1995).

F3. Downcore variation in XRD peak shape, p. 10.

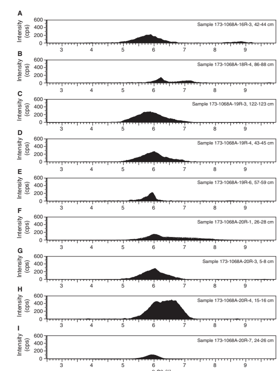

Relative variations in mineral abundances of the 3.04-Å calcite, 4.26-Å quartz, 4.03-Å plagioclase, 7.12-Å chlorite, 8.5-Å hornblende, 2.80-Å apatite, 5.6-Å analcime, 7.27-Å serpentine, and 3.06-Å garnet peaks are listed in Table T2. The mineral/boehmite peak area ratios for these minerals are plotted as a function of depth downcore in Figure F4. Matrix calcite generally decreases in abundance downcore, whereas the siliciclastic minerals (quartz and plagioclase), and minerals of diagenetic or hydrothermal origin (chlorite, analcime, and serpentine) show an increase in downcore abundance within the breccia matrix. The downcore transition from Maastrichtian Unit II marine sediments to the top of the Lower Cretaceous Unit IVA breccia (at 853 meters below seafloor [mbsf]) is marked by a sharp decrease in quartz, plagioclase, and chlorite abundances and a sharp increase in the abundance of calcite. Subunit IVA is generally characterized by a matrix with high calcite abundances and moderate abundances of quartz.

T2. Integrated intensity for Site 1068 matrix minerals and boehmite, p. 13.

F4. Mineral abundance for Site 1068 matrix minerals, p. 11.

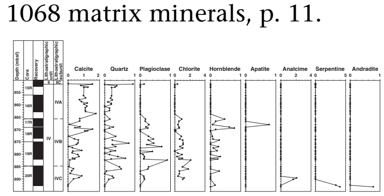

A change to generally lower and more variable calcite abundances, along with an increase in the noncalcareous minerals, occurs below 864 mbsf. This abundance change in the matrix mineralogy corresponds to (1) the transition from Subunit IVA to IVB, (2) an increase in fine rock fragments in the matrix (Shipboard Scientific Party, 1998), and (3) a color change of the powdered breccia matrix from predominantly moderate orange pink to variable browns, oranges, and grays (see Table T2). Apatite was present in only one sample (173-1068A-17R-2, 106–107 cm)(see the middle photo in Fig. F1 and also Fig. F2C) taken from a uniquely clast-poor, moderately sorted, 5-cm reddish brown to light brown layer within Subunit IVB that has a graded contact with the breccias above and below it. The clasts that are present in this interval are silt- to sand-size subrounded grains (Shipboard Scientific Party, 1998). The lithologic characteristics of the interval in which apatite is present do not support a hydrothermal origin for this mineral; shipboard description does not indicate the presence of a mineral vein from which the apatite could be derived.

Matrix chlorite, plagioclase, and quartz abundances are variable but generally increase downcore within Subunit IVB. The presence of these minerals may be attributed to hydrothermal alteration of the breccia matrix that increases in intensity with depth downcore. Alternatively, some portion of these minerals may be attributed to the inclusion of small rock fragments within the matrix or may have formed during diagenesis.

The downcore transition into Subunit IVC at 885 mbsf is marked by a decrease in quartz and plagioclase abundances. Other minerals do not show distinct abundance trends at this subunit boundary. However, below ~889.5 mbsf, a new suite of matrix minerals are present: analcime, serpentine, and andradite garnet. Analcime is a sodic zeolite of hydrothermal or diagenetic origin and the only zeolite stable in deeper, older rocks (Velde, 1995). Serpentine and garnet were identified shipboard in serpentinized peridotite immediately underlying the breccia succession (Shipboard Scientific Party, 1998). This study shows, however, that these minerals are also present in the deepest portion of the Subunit IVC breccia matrix.

ACKNOWLEDGMENTS

I sincerely appreciate Laura Combs' assistance with sample preparation. A helpful and constructive review was provided by Kitty Milliken. This work was funded by a JOI-USSSP postcruise research grant.

REFERENCES

Beard, J., and Hopkinson, L., in press. A fossil, serpentinization-related hydrothermal vent, ODP Leg 173, Site 1068 (Iberia Abyssal Plain): some aspects of mineral and fluid chemistry. *J. Geophys. Res.*

Bish, D.L., and Reynolds, R.C., Jr., 1989. Sample preparation for X-ray diffraction. *In* Bish, D.L., and Post, J.E. (Eds.), *Modern Powder Diffraction.* Rev. Mineral., 20:73–99.

Carroll, D., 1970. Clay minerals: a guide to their X-ray identification. *Spec. Pap.—Geol. Soc. Am.,* 126.

Comas, M.C., Sánchez-Gómez, M., Cornen, G., and de Kaenel, E., 1996. Serpentinized peridotite breccia and olistostrome on basement highs of the Iberia Abyssal Plain: implications for tectonic margin evolution. *In* Whitmarsh, R.B., Sawyer, D.S., Klaus, A., and Masson, D.G. (Eds.), *Proc. ODP, Sci. Results,* 149: College Station, TX (Ocean Drilling Program), 577–591.

Gibbs, R.J., 1967. Clay mineral segregation in the marine environment. *J. Sediment. Petrol.,* 47:237–243.

Gibson, I.L., Milliken, K.L., and Morgan, J.K., 1996. Serpentinite-breccia landslide deposits generated during crustal extension at the Iberia Margin. *In* Whitmarsh, R.B., Sawyer, D.S., Klaus, A., and Masson, D.G. (Eds.), *Proc. ODP, Sci. Results,* 149: College Station, TX (Ocean Drilling Program), 571–575.

Krissek, L.A., 1984. Continental source area contributions to fine-grained sediments on the Oregon and Washington continental slope. *In* Stow, D.A.V., and Piper, D.J.W. (Eds.), *Fine-grained Sediments: Deep Water Processes and Facies:* London (Blackwell Scientific), 363–375.

————, 1989. Bulk mineralogy of nonbiogenic sediments from ODP Sites 642 and 643, Norwegian Sea: implications for sediment provenance and recycling. *In* Eldholm, O., Thiede, J., Taylor, E., et al., *Proc. ODP, Sci. Results,* 104: College Station, TX (Ocean Drilling Program), 29–39.

Krissek, L.A., and Clemens, S.C., 1991. Mineralogic variations in a Pleistocene high-resolution Eolian record from the Owen Ridge, western Arabian Sea (Site 722): implications for sediment source conditions and monsoon history. *In* Prell, W.L., Niitsuma, N., et al., *Proc. ODP, Sci. Results,* 117: College Station, TX (Ocean Drilling Program), 197–213.

Krissek, L.A., and Janecek, T.R., 1993. Eolian deposition on the Ontong Java Plateau since the Oligocene: unmixing a record of multiple dust sources. *In* Berger, W.H., Kroenke, L.W., Mayer, L.A., et al., *Proc. ODP, Sci. Results,* 130: College Station, TX (Ocean Drilling Program), 471–490.

Scheidegger, K.F., and Krissek, L.A., 1982. Dispersal and deposition of eolian and fluvial sediments off Peru and northern Chile. *Geol. Soc. Am. Bull.,* 93:150–162.

Shipboard Scientific Party, 1994a. Site 897. *In* Sawyer, D.S., Whitmarsh, R.B., Klaus, A., et al., *Proc. ODP, Init. Repts.,* 149: College Station, TX (Ocean Drilling Program), 41–113.

————, 1994b. Site 899. *In* Sawyer, D.S., Whitmarsh, R.B., Klaus, A., et al., *Proc. ODP, Init. Repts.,* 149: College Station, TX (Ocean Drilling Program), 147–209.

————, 1998. Site 1068. *In* Whitmarsh, R.B., Beslier, M.-O., Wallace, P.J., et al., *Proc. ODP, Init. Repts.,* 173: College Station, TX (Ocean Drilling Program), 163–218.

Velde, B. (Ed.), 1995. *Origin and Mineralogy of Clays: Clays and the Environment:* Berlin (Springer-Verlag).

Whitmarsh, R.B., Beslier, M.-O., Wallace, P.J., et al., 1998. *Proc. ODP, Init. Repts.,* 173: College Station, TX (Ocean Drilling Program).

Figure F1. Downcore distribution of matrix mineralogy, Site 1068. Core photo examples of lithostratigraphic Subunits IVA (interval 173-1068A-16R-3, 70–90 cm), IVB (interval 173-1068A-17R-2, 85–108 cm), and IVC (interval 173-1068A-20R-1, 58–75 cm) are provided to the left of the qualitative mineralogical profile (core photos from Shipboard Scientific Party, 1998).

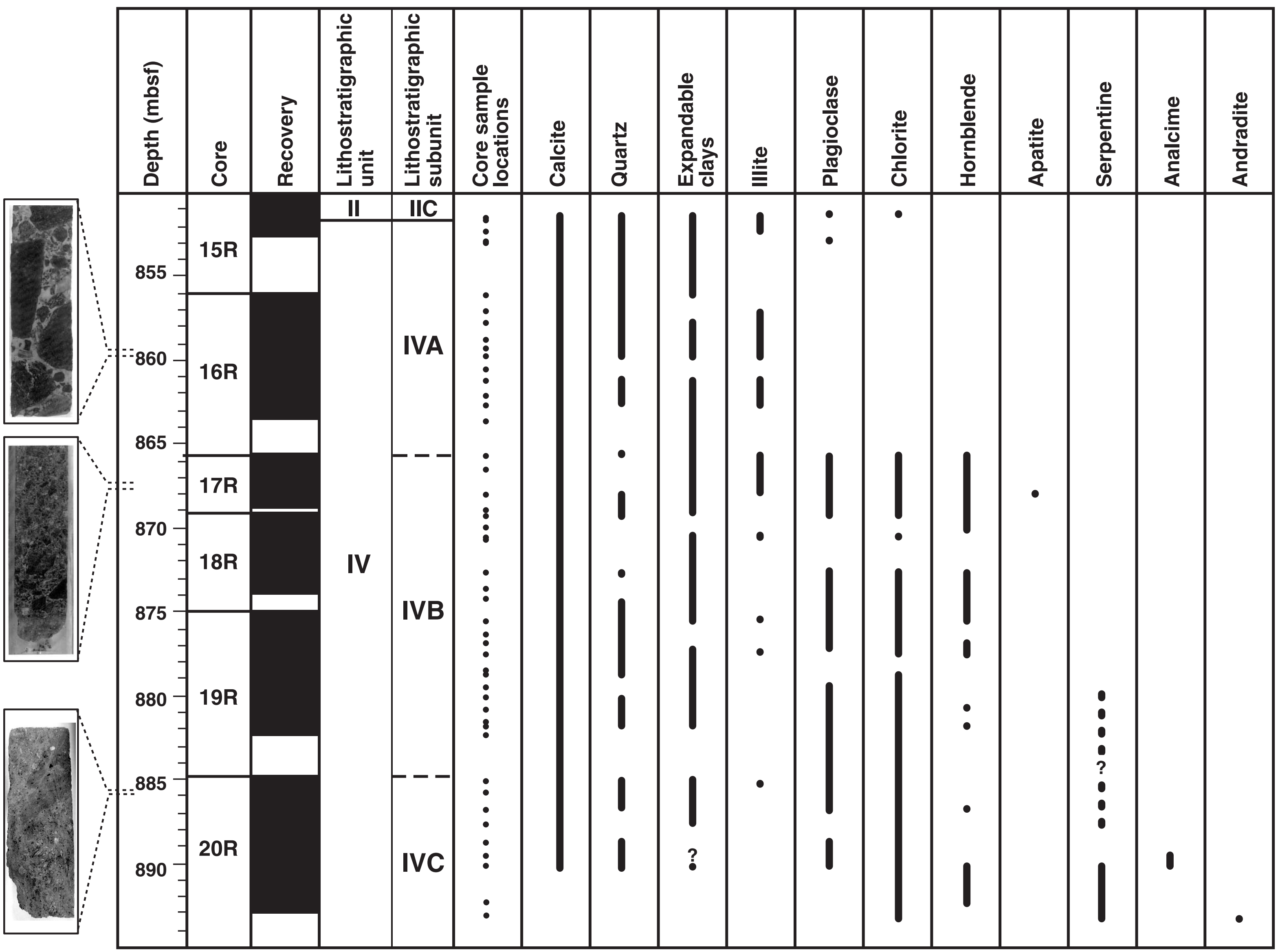

Figure F2. Example XRD profiles of six Site 1068 breccia matrix samples. **A.** Base of lithostratigraphic Unit II (851.55 mbsf). **B.** Subunit IVA (858.78 mbsf). **C.** Anomalous brown horizon within Subunit IVB (868.01 mbsf). I = peak intensity. Mineral identification is labeled above the corresponding peak. Note the difference in intensity scale between Figure F2 (A–C), p.8, and Figure F2 (D–F), p.9. Ch = chlorite, Cl = expandable clays, I = illite, B = boehmite, Q = quartz, P = plagioclase, Ca = calcite, H = hornblende, and Ap = apatite. cps = counts per second. (Continued on next page.)

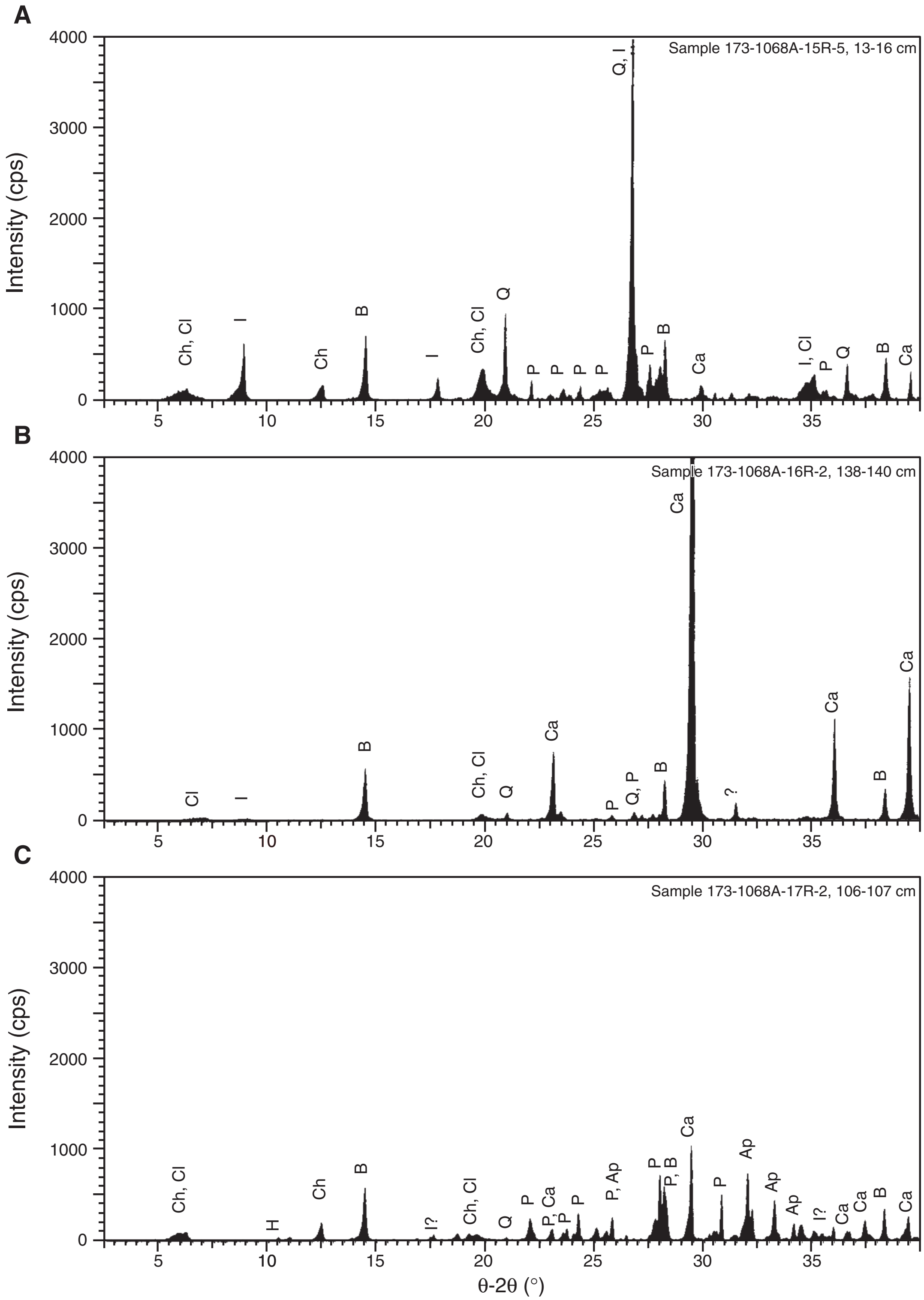

Figure F2 (continued). D. Subunit IVB (876.94 mbsf). **E.** Subunit IVC (890.08 mbsf). **F.** Subunit IVC (893.13 mbsf). An = analcime, S = serpentine, And = andradite.

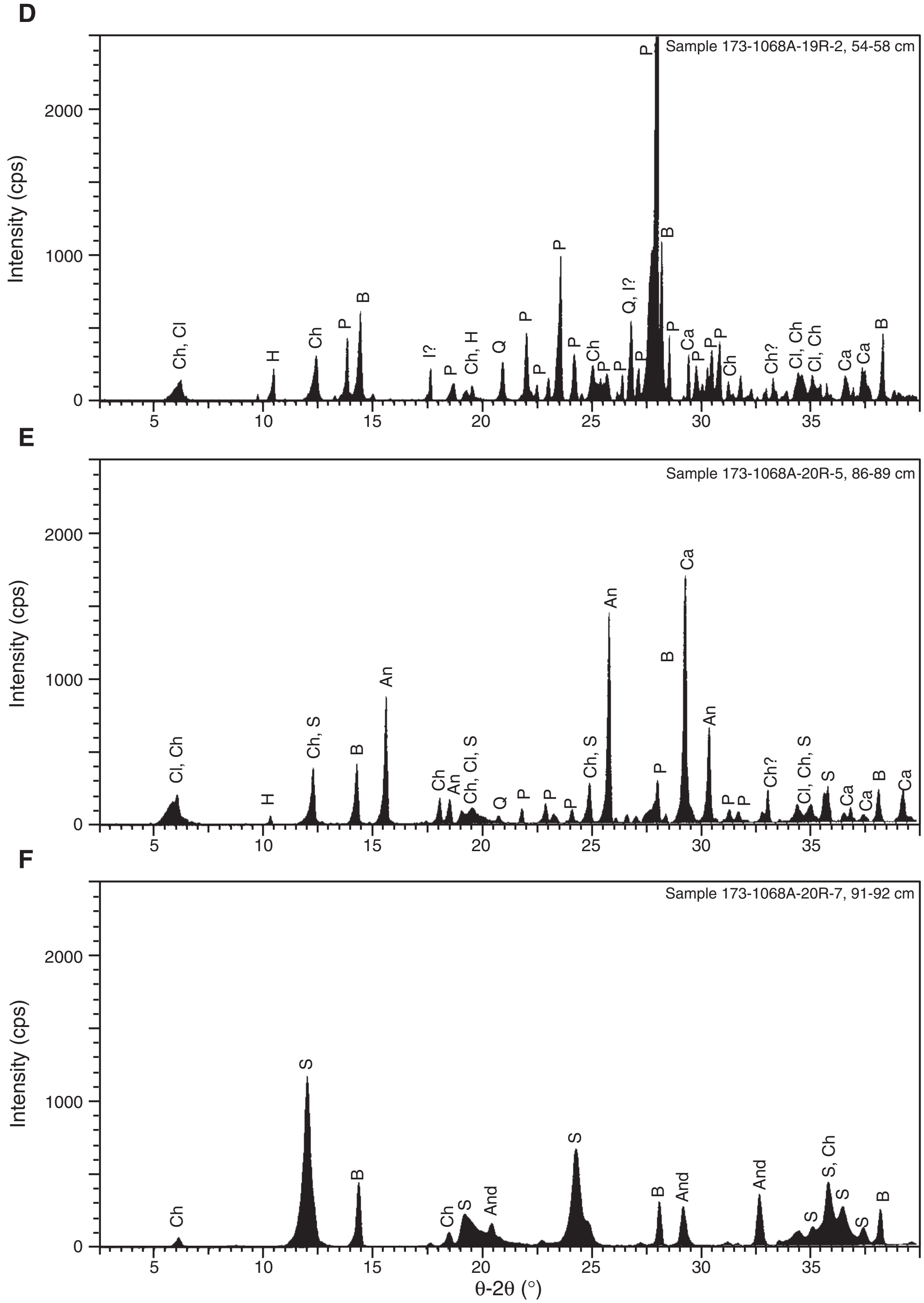

Figure F3. Example of the downcore variation in the shape of the 5°–7°2θ peak and the presence (or absence) of the 10-Å illite peak (8.8°2θ). The downcore variation in peak shape reflects a downcore variation in the type and abundance of expandable clay minerals in the breccia matrix. **A.** Lithostratigraphic Subunit IVA (859.32 mbsf). **B.** Subunit IVB (874.23 mbsf). **C.** Subunit IVB (878.80 mbsf). **D.** Subunit IVB (879.51 mbsf). **E.** Subunit IVB (882.33 mbsf). **F.** Subunit IVC (885.16 mbsf). **G.** Subunit IVC (886.72 mbsf). **H.** Subunit IVC (887.87 mbsf). **I.** Subunit IVC (992.46 mbsf).

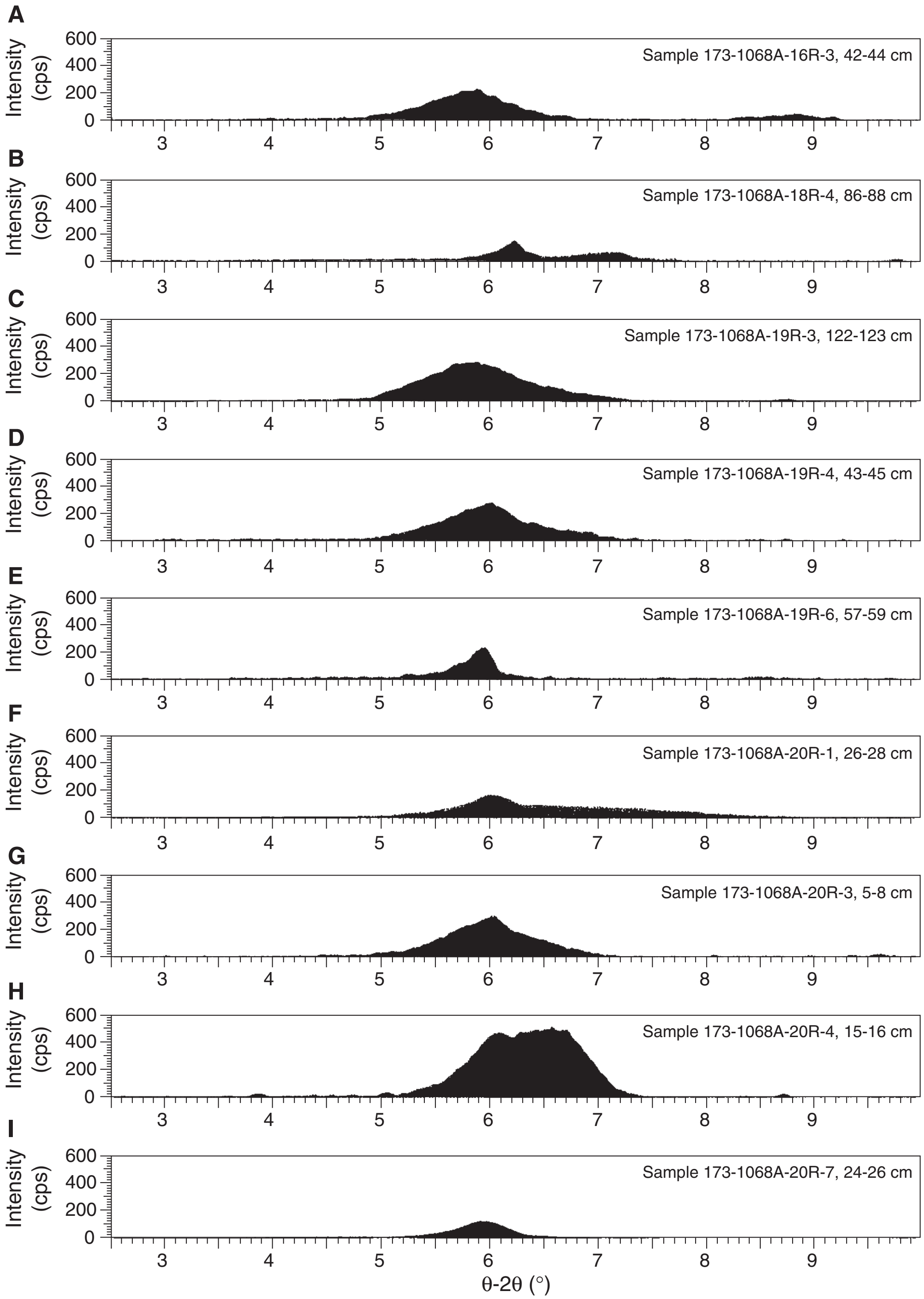

Figure F4. Mineral abundance data (mineral/boehmite integrated intensity ratios) for Site 1068 matrix minerals: calcite, quartz, plagioclase, chlorite, hornblende, apatite, analcime, serpentine, and andradite garnet, plotted as a function of downcore depth in meters below seafloor.

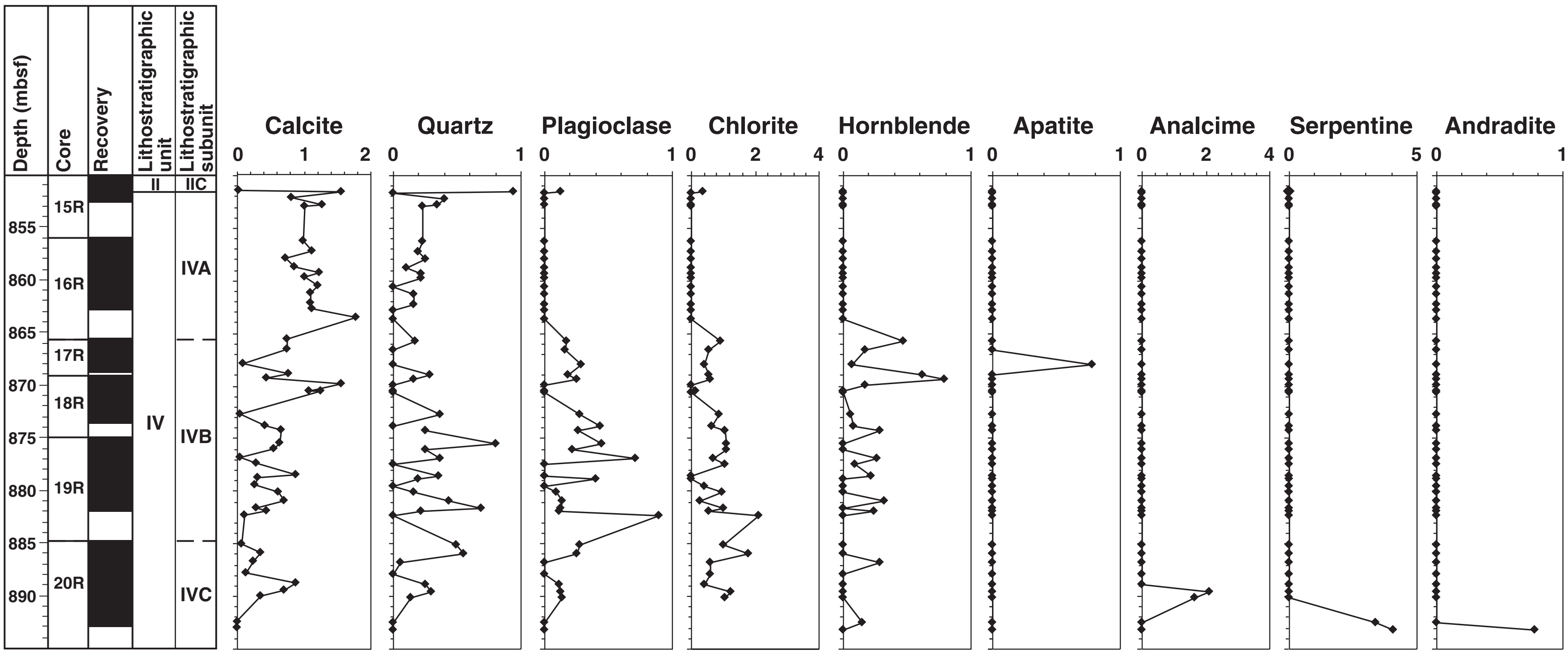

Table T1. Comparison between the bulk composition of the breccia subunits* and the results of this study.

Lithostratigraphic subunit	Bulk composition*	Matrix composition**
IVA	Calcite Plagioclase Chlorite Sericite?	Calcite Plagioclase Chlorite Quartz Illite Expandable clays
IVB	Calcite Plagioclase Chlorite Amphibole Quartz Goethite Ankerite	Calcite Plagioclase Chlorite Quartz Illite Expandable clays Hornblende Apatite Serpentine?
IVC	Calcite Plagioclase Chlorite Quartz Analcime	Calcite Plagioclase Chlorite Quartz Illite Expandable clays Hornblende Serpentine Analcime Andradite

Note: * = Shipboard Scientific Party, 1998; ** = this study.

Table T2. Integrated intensity (peak area) data for identified Site 1068 matrix minerals and for the internal standard, boehmite. (See table notes. Continued on next page.)

				Integrated intensities										
Core, section, interval (cm)	Depth (mbsf)	Munsell color	Powdered matrix color	2θ: d-spacing: Mineral:	14.4° 6.11 Å Boehmite	29.4° 3.04 Å Calcite	20.8° 4.26 Å Quartz	21.9° 4.03 Å Plagioclase	12.4° 7.12 Å Chlorite	10.3° 8.50 Å Hornblende	32.0° 2.80 Å Apatite	12.2° 7.27 Å Serpentine	15.8° 5.60 Å Analcime	29.2° 3.06 Å Andradite
173-1068A-														
15R-5, 13-15	851.55	5YR 5/6	Light brown		21,279	6,575	20,156	2,712	8,279					
15R-5, 20-22	851.62	5YR 8/4	Moderate orange pink		11,348	176,352	tr							
15R-5, 84-86	852.26	5YR 8/4	Moderate orange pink		18,770	154,422	7,659							
15R-6, 20-22	852.82	10YR 8/2	Very pale orange		15,980	203,166	5,458							
15R-6, 35-37	852.97	10YR 8/2	Very pale orange		15,975	163,175	3,605	tr						
16R-1, 36-37	856.26	10YR 8/6	Pale yellowish orange		17,377	172,527	4,004							
16R-1, 138-139	857.28	10YR 8/2	Very pale orange		11,116	124,874	2,216							
16R-2, 51-53	857.91	5YR 8/4	Moderate orange pink		21,870	160,717	5,450							
16R-2, 138-140	858.78	10YR 8/2	Very pale orange		17,953	152,407	1,912							
16R-3, 42-44	859.32	5YR 8/4	Moderate orange pink		15,833	196,233	3,522							
16R-3, 84-86	859.74	5YR 8/4	Moderate orange pink		18,196	183,723	3,940							
16R-4, 54-55	860.56	5YR 8/4	Moderate orange pink		15,273	183,905								
16R-4, 127-129	861.29	5YR 8/4	Moderate orange pink		17,445	191,796	2,873							
16R-5, 69-71	862.21	5YR 8/4	Moderate orange pink		16,681	183,821	2,732							
16R-5, 126-127	862.78	5YR 8/4	Moderate orange pink		15,683	175,980	tr							
16R-6, 58-61	863.60	10YR 8/2	Very pale orange		13,000	230,880								
17R-1, 10-14	865.70	10YR 6/2	Pale yellowish brown		9,268	68,377	1,633	1,634	8,337	4,384				
17R-1, 94-97	866.54	5Y 7/2	Yellowish gray		9,272	69,864		1,521	5,112	1,651				
17R-2, 106-107	868.01	5YR 5/6	Light brown		17,315	16,211	tr	5,049	7,102	1,100	1,3452			
17R-4, 146-149	869.00	10YR 7/4	Grayish orange		8,669	66,249	2,489	1,600	4,925	5,420				
18R-1, 18-20	869.38	5YR 6/4	Light brown		5,872	25,907	966	1,510	3,430	4,690				
18R-1, 71-74	869.91	10YR 8/6	Pale yellowish orange		11,463	178,770				1,957				
18R-2, 1-2	870.53	10YR 8/6	Pale yellowish orange		10,756	115,192			1,622					
18R-2, 9-13	870.61	5Y 7/2	Yellowish gray		10,194	126,662								
18R-3, 75-78	872.77	5Y 5/2	Light olive gray		8,496	3,298	3,152	2,337	7,386	503				
18R-4, -52-55	873.89	5Y 5/6	Light olive brown		14,960	63,346		6,480	9,954	1,283				
18R-4, 86-88	874.23	5YR 6/4	Light brown		13,348	87,779	3,353	3,541	14,103	3,778				
19R-1, 29-31	875.49	10YR 7/4	Grayish orange		5,134	32,903	4,143	2,327	5,604	tr				
19R-1, 91-93	876.11	5Y 7/2	Yellowish gray		10,924	59,639	2,751	2,412	12,290					
19R-2, 54-58	876.94	5Y 7/2	Yellowish gray		17,549	8,462	6,487	12,442	12,150	4,661				
19R-2, 100-102	877.40	10YR 6/6	Dark yellowish orange		12,355	36,454			12,856	1,127				
19R-3, 96-98	878.54	10YR 7/4	Grayish orange		9,544	84,617	3,369			2,076				
19R-3, 122-123	878.80	10YR 8/2	Very pale orange		13,148	40,343	2,591	5,319						
19R-4, 43-45	879.51	5Y 7/2	Yellowish gray		16,035	42,912		tr	6,910					
19R-4, 106-108	880.14	5Y 7/2	Yellowish gray		12,056	73,063	1,877	1,132	11,873					
19R-5, 44-46	880.98	10YR 7/4	Grayish orange		7,446	52,542	3,215	1,040	2,222	2,411				
19R-5, 111-113	881.65	10YR 6/6	Dark yellowish orange		11,721	32,967	8,028	1,440	11,642					
19R-6, 16-17	881.92	10YR 6/6	Dark yellowish orange		9,361	41,568	1,991	1,044	5,139	2,291				
19R-6, 57-59	882.33	5Y 7/2	Yellowish gray		10,781	11,509		9,651	22,743					
20R-1, 26-28	885.16	10Y 8/2	Pale greenish yellow		13,946	8,437	6,948	3,775	14,255					
20R-2, 13-15	885.88	10Y 8/2	Pale greenish yellow		6,634	23,558	3,635	1,711	11,801					
20R-3, 5-8	886.72	5Y 7/2	Yellowish gray		14,538	36,680	845		84,31	4,247				
20R-4, 15-16	887.87	5Y 7/2	Yellowish gray		23,958	32,570			14,097					
20R-4, 12-116	888.84	N9	White		11,728	102,080	2,900	1,305	4,843					
20R-5, 34-36	889.56	5Y 8/4	Grayish yellow		7,911	54,799	2,406	1,036	9,820				16,619	

Table T2 (continued).

					Integrated intensities										
				2θ:	14.4°	29.4°	20.8°	21.9°	12.4°	10.3°	32.0°	12.2°	15.8°	29.2°
				d-spacing:	6.11 Å	3.04 Å	4.26 Å	4.03 Å	7.12 Å	8.50 Å	2.80 Å	7.27 Å	5.60 Å	3.06 Å
Core, section, interval (cm)	Depth (mbsf)	Munsell color	Powdered matrix color	Mineral:	Boehmite	Calcite	Quartz	Plagioclase	Chlorite	Hornblende	Apatite	Serpentine	Analcime	Andradite
20R-5, 86-89	890.08	5B 9/1	Bluish white		13,204	47,067	1,791	1,811	13,740				21,614	
20R-7, 24-26	892.46	5GY 8/1	Light greenish gray		18,416				?	2,661		62,919		
20R-7, 91-92	893.13	5GY 8/1	Light greenish gray		14,724				?			60,046		11,409

Notes: Depth in meters below seafloor (mbsf) indicates top of sample. Peaks that were identified but were too small to calculate their integrated intensities are labeled as occurring in trace amounts (tr).